Magnetic-Field Transmission Through a Circular Aperture in a Magneto-Conductive Screen: Identification of Aperture Penetration and Field Diffusion Contributions

Giampiero Lovat, Paolo Burghignoli, *Senior Member, IEEE*, Rodolfo Araneo, *Senior Member, IEEE*, and Salvatore Celozzi, *Senior Member, IEEE*

***Abstract*—The magnetic field transmitted through a circular aperture in an infinite magneto-conductive planar screen with finite thickness is studied, considering as a source a circular electric current loop coaxial with the aperture. The field source consists of a circular electric current loop coaxial with the aperture. First, the finite thickness of the aperture is taken into account through suitable generalized boundary conditions. Next, a pair of dual integral equations are obtained whose solutions are obtained by means of an expansion of the unknowns in Neumann series of Bessel functions combined with a Galerkin method of moments. Such solutions furnish equivalent electric and magnetic spectral current densities from which all the field components can easily be obtained. The proposed formulation allows for clearly distinguishing the contributions to the total transmitted field coming from the diffusion in the magneto-conductive screen and the penetration through the aperture, thus gaining physical insight into the transmission mechanism. Numerical results are presented and compared with those obtained through commercial software to show the accuracy and the efficiency of the proposed formulation.**

***Index Terms*—Apertures, conductivity, diffusion, electromagnetic shielding, finite thickness, near field.**

I. Introduction

THE transmission of the electromagnetic field through a circular aperture in an infinite perfectly conducting (PEC) plane with infinitesimal thickness is a canonical problem which admits an exact solution in terms of oblate spheroidal vector wavefunctions, after solving the complementary disk problem [1]. Under the assumption of small aperture, different approximate formulations have also been proposed based on electrostatic and magnetostatic approximations of the fields at the aperture [2], [3] or, starting from a rigorous spectral-domain approach, considering the limiting cases of near and/or far-field regions [4], [5]. In [6], the case of a circular electric current loop has instead been addressed through the solution of a second-kind Fredholm integral equation and the application of the Abel integral-transform technique. As said above, most of the works in the literature consider the case of a circular aperture in a PEC plane, i.e., a conducting plane with an ideal infinite electric conductivity. In fact, in such a case, the Babinet principle can be applied and the scattering problem from an aperture in a PEC plane can thus be reduced to the scattering problem from a PEC disk [7], [8]. Other approaches apply the equivalence principle to derive an integral equation whose unknown is the equivalent magnetic current density on the metalized aperture [6].

On the other hand, the diffraction of plane waves from a circular aperture with finite thickness in a PEC plate has been investigated in [9] using the so-called coupled-mode method and, more recently, in [10] through a boundary element method and in [11] using a theory based on the eigenvector expansion and mode matching. Only in connection with the extraordinary optical transmission phenomenon, the diffraction of light from a single aperture in nonideal thick metals (characterized by a complex dielectric constant) has started to be analyzed [12], [13].

In this work, we present an original formulation for the evaluation of the field generated by a circular current loop and transmitted through a circular aperture (coaxial with the loop) cut in a planar magneto-conductive screen of finite thickness. To the best of our knowledge, this practical problem has never been rigorously addressed in the literature, although the aperture in a PEC plate [6], [14] and the infinite planar conductive and magnetic screen [15], [16], [17], [18], [19], [20] have been extensively studied.

Only very recently, the problem of the electromagnetic field penetration through a circular aperture in a infinitesimally-thin plate characterized by a *nonzero surface impedance* has been addressed through a dual-integral-equation approach [21]. In this work, with respect to [21], the finite thickness of the aperture, the finite conductivity and the permeability of the plate are taken into account through suitable generalized boundary conditions.

Manuscript received 8 February 2023; revised 19 April 2023; accepted 13 May 2023. *(Corresponding author: Giampiero Lovat.)*

Giampiero Lovat, Rodolfo Araneo, and Salvatore Celozzi are with the Electrical Engineering Division of DIAEE, University of Rome "Sapienza", 00184 Rome, Italy (e-mail: giampiero.lovat@uniroma1.it; rodolfo.araneo@uniroma1.it; salvatore.celozzi@uniroma1.it).

Paolo Burghignoli is with the Department of Information Engineering, Electronics and Telecommunications, University of Rome "Sapienza", 00184 Rome, Italy (e-mail: paolo.burghignoli@uniroma1.it).

Color versions of one or more figures in this article are available at https://doi.org/10.1109/TEMC.2023.3277028.

Digital Object Identifier 10.1109/TEMC.2023.3277028

Next, a pair of dual integral equations are derived whose solutions are obtained by a Galerkin method of moments in the Hankel spectral domain in which the unknowns are expanded in Neumann series of Bessel functions. Such solutions furnish equivalent electric and magnetic spectral current densities from which all the field components can easily be obtained through suitable inverse Hankel-transform integrals. It is worth mentioning that in [21], only one pair of dual integral equations was sufficient to describe the problem and the unknown was the spectral electric current density on the impedance plate. On the other hand, in the configuration analyzed in the present article, both electric and magnetic current densities need to be introduced making the problem more complex. However, we show that by decomposing the current loop source into even- and odd-symmetric parts, two subproblems can be derived and the relevant pairs of dual integral equations are decoupled. In this framework, [21] is a particular case of the more general problem considered here, which reduces to the problem considered in [21] for nonmagnetic screens with small thicknesses (smaller than the skin depth) and suitably low frequencies.

On the other hand, the use of the adopted generalized boundary conditions limits the analysis to subwavelength thicknesses: The the proposed formulation has thus an upper limit in frequency $f_{\max}$ depending on the screen thickness d (in particular $f_{\max} \simeq c/(2\,d)$, where c is the speed of light in free space). However, it should be noted that all the practical configurations (metallic and/or magnetic screens up to the microwave range) remain well inside this class of structures. In addition, we want to mention a possible limitation of the present study: In fact, for simplicity, the electric current in the loop is assumed to be constant. In principle, the extension of the proposed analysis to nonconstant currents could be feasible, but introducing an azimuthal dependence of the exciting current would destroy the azimuthal invariance of the problem, thereby making the incident and scattered field hybrid. We leave this analysis for a future work. We point out that the analysis presented here is limited to apertures of circular shape: this assumption allows for simplifying the numerical treatment of the problem, taking advantage of the azimuthal symmetry and of the possibility of expanding the unknowns of the integral equations through entire-domain basis functions. Again, the consideration of more complex shapes could be feasible using, e.g., an expansion in a Fourier series to take into account the azimuthal dependence of the problem and an expansion of the unknowns in RWG subdomain basis functions to model the arbitrary shape of the aperture. However, the assumption of circular aperture, while maintaining a numerical simplicity, allows for deriving general considerations on the involved electromagnetic phenomena. Finally, a last limitation of the proposed analysis consists in considering screens of infinite extent: It is understood that such an assumption does not allow for taking into account possible edge diffraction effects from the edges of the screen: However, the latter should be negligible for sufficiently large screens (with respect to the operating wavelength).

One great advantage of the proposed formulation consists also in the possibility of separating the contributions to the total transmitted field coming from the diffusion in the magneto-conductive screen and the penetration through the aperture, thus gaining physical insight into the transmission mechanism.

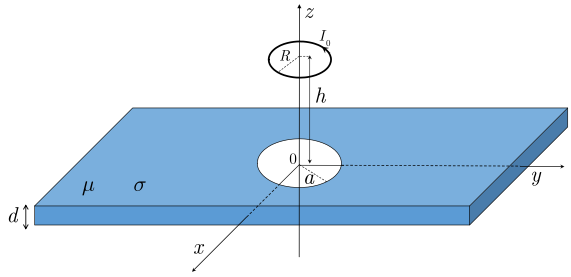

Fig. 1. Configuration under analysis: Infinite conductive plate characterized by a conductivity σ, a magnetic permeability μ, and a finite thickness d with a circular aperture of radius a in the presence of a coaxial current loop of radius R and constant current I_0 (coaxial with the aperture) placed at a distance h from it.

The rest of this article is organized as follows. The problem is described in Section II, where the adopted GBCs are also discussed and two auxiliary subproblems are introduced, each of which leads to a dual integral equation whose unknown is an equivalent spectral electric or magnetic current density. The procedure for the solution of this pair of dual integral equations is outlined in Section III, where all the quantities of interest are also calculated. As mentioned above, the proposed formulation allows for clearly distinguishing the contributions of the infinite solid screen and the aperture. Numerical results are presented in Section IV to show the accuracy and the efficiency of the proposed approach and to point out possible critical situations in particular configurations. Finally, Section V concludes the article.

II. Formulation of the Problem

The configuration under analysis is reported in Fig. 1 and it consists of an infinite conductive plate characterized by a conductivity σ, a magnetic permeability $\mu = \mu_0\mu_{\rm r}$, a finite thickness d, and symmetrically placed around the plane $z = 0$ of a cylindrical coordinate system (ρ, ϕ, z). A circular aperture of radius a is cut in it with center at the origin and a current loop of radius R and constant current I_0 (coaxial with the aperture) is placed at a distance h from it with a time-harmonic $\mathrm{e}^{\mathrm{j}\omega t}$ behavior. Such a source produces a purely incident TE_z field with nonzero components $E_\phi^{\rm inc}$, $H_\rho^{\rm inc}$, and $H_z^{\rm inc}$.

A. Generalized Boundary Conditions

The finite thickness of the screen makes the analysis more complex with respect to the infinitesimally-thin structure case. However, if the thickness d is sufficiently small (in particular, $k_0 d \ll 1$, where k_0 is the free-space wavenumber), it is possible to shrink the thickness to zero and adopt generalized boundary conditions (GBCs), which relate the tangential average electric (magnetic) fields to the tangential magnetic (electric) field jump across an infinitely thin surface, i.e.,

$$\frac{1}{2}\left[E_\phi\left(\rho, z = 0^+\right) + E_\phi\left(\rho, z = 0^-\right)\right]$$

$$= \zeta_0 \hat{Z}_S \left(\mathbf{u}_z \times \mathbf{u}_\rho\right) \left[H_\rho\left(\rho, z=0^+\right) - H_\rho\left(\rho, z=0^-\right)\right] \quad (1)$$

and

$$\frac{1}{2}\left[H_\rho\left(\rho, z=0^+\right) + H_\rho\left(\rho, z=0^-\right)\right] = -\frac{\hat{Y}_S}{\zeta_0}\left(\mathbf{u}_z \times \mathbf{u}_\phi\right)\left[E_\phi\left(\rho, z=0^+\right) - E_\phi\left(\rho, z=0^-\right)\right] \quad (2)$$

where ζ_0 is the free-space impedance. Such GBCs have recently be used successfully in different scattering problems [22], [23], [24], [25], [26].

The coefficients $\hat{Z}_S$ and $\hat{Y}_S$ are related to the thickness and the electromagnetic parameters of the screen and different expressions have been proposed in the literature. In his seminal paper [27], Mitzner derived

$$\hat{Z}_{SM} = \mathrm{j}\frac{\zeta_{\mathrm{cr}}}{2}\cot\left(\frac{k_{\mathrm{c}} d}{2},\right), \qquad \hat{Y}_{SM} = \mathrm{j}\frac{1}{2\zeta_{\mathrm{cr}}}\cot\left(\frac{k_{\mathrm{c}} d}{2}\right) \quad (3)$$

with

$$k_{\mathrm{c}} = k_0\sqrt{\mu_{\mathrm{r}}\varepsilon_{\mathrm{cr}}}, \qquad \zeta_{\mathrm{cr}} = \sqrt{\frac{\mu_{\mathrm{r}}}{\varepsilon_{\mathrm{cr}}}} \quad (4)$$

where $\varepsilon_{\mathrm{cr}} = 1 - \mathrm{j}\sigma/(\omega\varepsilon_0)$ indicates the relative complex permittivity.

More recently, Karlsson [28] proposed more refined expressions which take into account the compensation for the reduction of the screen volume to a surface of infinitesimal thickness and which lead to more accurate results, i.e.,

$$\hat{Z}_{SK} = \frac{\eta - \hat{Z}_{SM}\left(1+\eta^2\right)}{4\eta\hat{Z}_{SM} - \left(1+\eta^2\right)}, \qquad \hat{Y}_{SK} = \frac{\eta - \hat{Y}_{SM}\left(1+\eta^2\right)}{4\eta\hat{Y}_{SM} - \left(1+\eta^2\right)} \quad (5)$$

where

$$\eta = \mathrm{j}\cot\left(\frac{k_0 d}{4}\right). \quad (6)$$

It is worth noting that the condition $k_0 d \ll 1$ is not a limiting factor in all the practical configurations, where the thickness d of the screen is much smaller than the operating wavelength up to the microwave range.

B. Decomposition Into Even- and Odd-Symmetric Subproblems

The GBCs in (1) and (2) define a *combined electrically resistive/magnetically conductive sheet* with infinitesimal thickness, which supports both electric and magnetic surface currents, related to the discontinuities across the sheet of the tangential magnetic and electric fields, respectively. Since any plane containing the vertical z-axis is an odd symmetry plane, the electric surface current density $\mathbf{J}_{\mathrm{s}}$ is azimuthally directed, whereas the magnetic current density $\mathbf{M}_{\mathrm{s}}$ is radially directed (see Fig. 2).

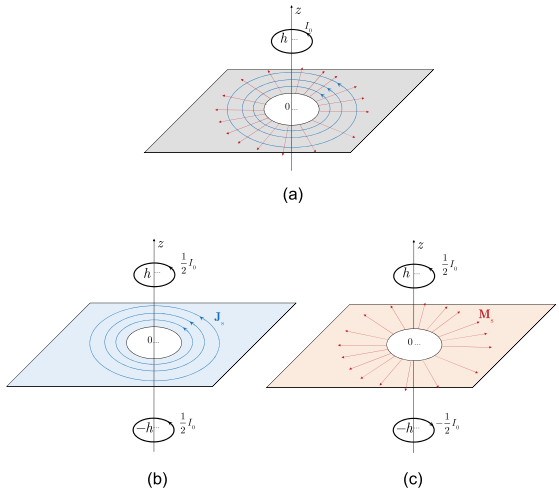

Fig. 2. (a) Combined electrically resistive/magnetically conductive infinitesimally thin sheet used to model the screen in Fig. 1, excited by a loop of electric current, and the relevant decomposition into even-symmetric, (b) and odd-symmetric (c) and configurations.

Electric and magnetic current densities defined over curved surfaces generally interact (i.e., the field produced by one of the currents couple to the other current). However, for a planar sheet, the reflection symmetry of the configuration with respect to the normal z-axis makes the two currents uncoupled [29]. The problem can thus be conveniently decoupled into two distinct subproblems; for instance, by decomposing the original electric current loop source into even- and odd-symmetric parts, the former is readily seen to excite only electric currents on the sheet, whereas the latter excites only magnetic currents, as shown in Fig. 2(b) and (c), respectively.

In the following subsections, the two subproblems will be separately discussed.

C. Even-Symmetric Subproblem

The boundary condition on the plate for the even-symmetry subproblem is

$$E_\phi^{(1)\mathrm{scat}}\left(\rho, z=0\right) + E_\phi^{(1)\mathrm{inc}}\left(\rho, z=0\right) = \zeta_0 \hat{Z}_S J_{S\phi}\left(\rho\right) \quad (7)$$

where

$$J_{S\phi}\left(\rho\right) = 0, \qquad \rho < a\,. \quad (8)$$

The incident field $E_\phi^{(1)\mathrm{inc}}$ is that produced by the original current loop of current $I_0/2$ at $z = h$ and by its mirror image at $z = -h$ in free space, i.e.,

$$E_\phi^{(1)\mathrm{inc}}\left(\rho, z\right) = -\frac{k_0\zeta_0 I_0 R}{4a} \cdot \int_0^\infty \frac{\mathrm{e}^{-\mathrm{j}\lambda|z-h|/a} + \mathrm{e}^{-\mathrm{j}\lambda|z+h|/a}}{\lambda} \mathrm{J}_1\left(\nu\frac{R}{a}\right)\mathrm{J}_1\left(\nu\frac{\rho}{a}\right)\nu\,\mathrm{d}\nu \quad (9)$$

where ν is the normalized radial wavenumber, $\mathrm{J}_1(\cdot)$ is the Bessel function of order 1, and

$$\lambda = \sqrt{(k_0 a)^2 - \nu^2}$$

is the z-component of the normalized spectral wavenumber. The scattered field $E_\phi^{(1)\mathrm{scat}}$ is that radiated by the electric current density $J_{S\phi}$ induced on the screen, i.e.,

$$E_\phi^{(1)\mathrm{scat}}(\rho, z) = -\frac{k_0\zeta_0}{2a}\int_0^\infty \tilde{J}_{S\phi}\left(\frac{\nu}{a}\right)\frac{\mathrm{e}^{-\mathrm{j}\lambda|z|/a}}{\lambda}\mathrm{J}_1\left(\nu\frac{\rho}{a}\right)\nu\,\mathrm{d}\nu \quad (10)$$

where $\tilde{J}_{S\phi}(\nu/a)$ is the Hankel transform of order 1 of the surface current density $J_{S\phi}(\rho)$.

Using (9), (10), and expressing the electric current density $J_{S\phi}(\rho)$ as an inverse Hankel transform

$$J_{S\phi}(\rho) = \frac{1}{a^2}\int_0^\infty \tilde{J}_{S\phi}\left(\frac{\nu}{a}\right)\mathrm{J}_1\left(\frac{\nu}{a}\rho\right)\nu\,\mathrm{d}\nu \quad (11)$$

and rearranging some terms, (7) and (8) can be rewritten as a first pair of dual integral equations as

$$\int_0^\infty \left(\frac{k_0 a}{2\lambda} + \hat{Z}_S\right)\tilde{J}_{S\phi}\left(\frac{\nu}{a}\right)\mathrm{J}_1(\nu r)\,\nu\,\mathrm{d}\nu = -\frac{I_0 k_0 a R}{2}\int_0^\infty \frac{\mathrm{e}^{-\mathrm{j}\lambda|h|/a}}{\lambda}\mathrm{J}_1\left(\nu\frac{R}{a}\right)\mathrm{J}_1(\nu r)\,\nu\,\mathrm{d}\nu, r > 1 \quad (12)$$

$$\int_0^\infty \tilde{J}_{S\phi}\left(\frac{\nu}{a}\right)\mathrm{J}_1(\nu r)\,\nu\,\mathrm{d}\nu = 0, \quad r < 1 \quad (13)$$

where $r = \rho/a$ and the spectral current $\tilde{J}_{S\phi}$ is the unknown function. Once the spectral electric current is known, any component of the scattered field $E_\phi^{(1)\mathrm{scat}}$, $H_\rho^{(1)\mathrm{scat}}$, and $H_z^{(1)\mathrm{scat}}$ can be calculated through a suitable inverse Hankel-transform integral [30].

D. Odd-Symmetric Subproblem

Dually, the boundary condition on the plate for the odd-symmetry subproblem is

$$H_\rho^{(2)\mathrm{scat}}(\rho, z=0) + H_\rho^{(2)\mathrm{inc}}(\rho, z=0) = \frac{\hat{Y}_S}{\zeta_0}M_{S\rho}(\rho) \quad (14)$$

where

$$M_{S\rho}(\rho) = 0, \qquad \rho < a\,. \quad (15)$$

The incident field $H_\rho^{(2)\mathrm{inc}}$ is that produced by the original current loop with current $I_0/2$ at $z = h$ and by its antimirror image with current $-I_0/2$ at $z = -h$ in free space, i.e.,

$$H_\rho^{(2)\mathrm{inc}}(\rho, z) = -\frac{I_0 R}{4a^2}\cdot\int_0^\infty\left(\mathrm{e}^{-\mathrm{j}\lambda|z-h|/a} + \mathrm{e}^{-\mathrm{j}\lambda|z+h|/a}\right)\mathrm{J}_1\left(\nu\frac{R}{a}\right)\mathrm{J}_1\left(\frac{\nu}{a}\rho\right)\nu\,\mathrm{d}\nu \quad (16)$$

while the scattered field $H_\rho^{(2)\mathrm{scat}}$ is that radiated by the magnetic current density $M_{S\rho}$ induced on the screen, i.e.,

$$H_\rho^{(2)\mathrm{scat}}(\rho, z) = -\frac{1}{2k_0\zeta_0 a^3}\int_0^\infty \lambda\,\mathrm{e}^{-\mathrm{j}\lambda|z|/a}\tilde{M}_{S\rho}\left(\frac{\nu}{a}\right)\mathrm{J}_1\left(\frac{\nu}{a}\rho\right)\nu\,\mathrm{d}\nu \quad (17)$$

where $\tilde{M}_{S\rho}(\nu/a)$ is the Hankel transform of order 1 of the surface current density $M_{S\rho}(\rho)$.

Using (16), (17), and by expressing the magnetic current density $M_{S\rho}(\rho)$ as an inverse Hankel transform

$$M_{S\rho}(\rho) = \frac{1}{a^2}\int_0^\infty \tilde{M}_{S\rho}\left(\frac{\nu}{a}\right)\mathrm{J}_1\left(\frac{\nu}{a}\rho\right)\nu\,\mathrm{d}\nu \quad (18)$$

and rearranging some terms, (14) and (15) can be rewritten as a second pair of dual integral equations as

$$\int_0^\infty \left(\frac{\lambda}{2k_0 a} + \hat{Y}_S\right)\tilde{M}_{S\rho}\left(\frac{\nu}{a}\right)\mathrm{J}_1(\nu r)\,\nu\,\mathrm{d}\nu = -\frac{I_0 R\zeta_0}{2}\int_0^\infty \mathrm{e}^{-\mathrm{j}\lambda|h|/a}\mathrm{J}_1\left(\nu\frac{R}{a}\right)\mathrm{J}_1(\nu r)\,\nu\,\mathrm{d}\nu, r > 1 \quad (19)$$

$$\int_0^\infty \tilde{M}_{S\rho}\left(\frac{\nu}{a}\right)\mathrm{J}_1(\nu r)\,\nu\,\mathrm{d}\nu = 0, \quad r < 1 \quad (20)$$

where the spectral current $\tilde{M}_{S\rho}$ is the unknown function. Once the spectral magnetic current is known, any component of the scattered field $E_\phi^{(2)\mathrm{scat}}$, $H_\rho^{(2)\mathrm{scat}}$, and $H_z^{(2)\mathrm{scat}}$ can be calculated through a suitable inverse Hankel-transform integral [30].

III. Solution of the Dual Integral Equations

The dual integral (12), (13) and (19), (20) are both in the same form as those studied in [21]. In particular, they can both be reduced to the canonical form

$$\int_0^\infty \gamma_i(\nu)\,\psi_i(\nu)\,\mathrm{J}_1(\nu r)\,\mathrm{d}\nu = q_i(r), \qquad 0 < r < 1 \quad (21)$$

$$\int_0^\infty \psi_i(\nu)\,\mathrm{J}_1(\nu r)\,\mathrm{d}\nu = 0, \qquad r > 1 \quad (22)$$

where $i = 1$ and $i = 2$ denote the even-symmetrical and odd-symmetrical problem, respectively, and

$$\gamma_i(\nu) = \frac{\alpha_i(\nu)}{\beta_i(\nu)}, \quad (23)$$

$$\psi_i(\nu) = \beta_i(\nu)\,f_i(\nu) - \nu G_i(\nu) \quad (24)$$

and

$$q_i(r) = -\int_0^\infty \nu G_i(\nu)\,\gamma_i(\nu)\,\mathrm{J}_1(\nu r)\,\mathrm{d}\nu\,. \quad (25)$$

In particular, for the even-symmetry subproblem $i = 1$ we have

$$f_1(\nu) = \tilde{J}_{S\phi}\left(\frac{\nu}{a}\right), \quad (26)$$

$$\alpha_1(\nu) = \nu\,, \quad (27)$$

$$\beta_1(\nu) = \nu\left(\frac{k_0 a}{2\lambda} + \hat{Z}_S\right) \tag{28}$$

and

$$G_1(\nu) = -\frac{I_0 k_0 a R}{2}\,\frac{\mathrm{e}^{-\mathrm{j}\lambda h/a}}{\lambda}\,\mathrm{J}_1\left(\nu\frac{R}{a}\right) \tag{29}$$

whereas for the odd-symmetry problem $i = 2$ it results

$$f_2(\nu) = \tilde{M}_{S\rho}\left(\frac{\nu}{a}\right), \tag{30}$$

$$\alpha_2(\nu) = \nu, \tag{31}$$

$$\beta_2(\nu) = \nu\left(\frac{\lambda}{2k_0 a} + \hat{Y}_S\right) \tag{32}$$

and

$$G_2(\nu) = -\frac{I_0 R \zeta_0}{2}\,\mathrm{e}^{-\mathrm{j}\lambda h/a}\,\mathrm{J}_1\left(\nu\frac{R}{a}\right). \tag{33}$$

As described in [21], in order to solve the dual integral (21), (22), the $\psi(\nu)$ function (which is related either to the $\tilde{J}_{S\phi}$ or to the $\tilde{M}_{S\rho}$ functions) is expanded in a Neumann series of Bessel functions, i.e,

$$\psi_i(\nu) = \nu^{1-\mu_i}\sum_{n=0}^{+\infty}\psi_n^{(i)}\mathrm{J}_{2n+1+\mu_i}(\nu)\,. \tag{34}$$

In fact, thanks to the well-known discontinuous Sonine–Schafheitlin integral [31, 6.574.3]

$$\int_0^\infty x^{1-\mu_i}\mathrm{J}_{2n+1+\mu_i}(x)\mathrm{J}_1(xy)\,\mathrm{d}x = 0 \qquad y > 1\,,\mu_i > 0 \tag{35}$$

Equation (34) automatically satisfies (22). The parameter μ_i in (34) is arbitrary (provided that $\mu_i > 0$) and can be used to guarantee the convergence of the integrals arising in the analysis or to enforce a specific order of singularity of the spatial currents at the edge of the aperture [21]. Using the expansion (34) and following the same steps as in [21], the dual integral equations are reduced to the matrix system

$$\sum_{n=0}^{+\infty} A_{mn}^{(i)}\psi_n^{(i)} = U_m^{(i)}, \qquad m = 0, 1, \ldots \tag{36}$$

where the matrix elements are given by

$$A_{mn}^{(i)} = \int_0^\infty \nu^{1-2\mu_i}\gamma_i(\nu)\,\mathrm{J}_{2m+1+\mu_i}(\nu)\,\mathrm{J}_{2n+1+\mu_i}(\nu)\,\mathrm{d}\nu \tag{37}$$

and

$$U_m^{(i)} = -\int_0^\infty \nu^{1-\mu_i}\gamma_i G_i(\nu)(\nu)\,\mathrm{J}_{2m+1+\mu_i}(\nu)\,\mathrm{d}\nu\,. \tag{38}$$

From (37), and the expressions of $\gamma_i(\nu)$ it is easy to derive that it must be $\mu_1 > 1/2$ and $\mu_2 > 0$, so that we can set $\mu_1 = \mu_2 = 1$ and therefore

$$A_{mn}^{(i)} = \int_0^\infty \frac{\gamma_i(\nu)}{\nu}\,\mathrm{J}_{2m+2}(\nu)\,\mathrm{J}_{2n+2}(\nu)\,\mathrm{d}\nu \tag{39}$$

and

$$U_m^{(i)} = -\int_0^\infty G_i(\nu)\,\gamma_i(\nu)\,\mathrm{J}_{2m+2}(\nu)\,\mathrm{d}\nu\,. \tag{40}$$

Equations (39) and (40) can explicitly be written as

$$A_{mn}^{(1)} = \int_0^\infty \frac{\lambda}{\nu\left(k_0 a + 2\lambda\hat{Z}_S\right)}\,\mathrm{J}_{2m+2}(\nu)\,\mathrm{J}_{2n+2}(\nu)\,\mathrm{d}\nu\,, \tag{41}$$

$$A_{mn}^{(2)} = \int_0^\infty \frac{1}{\nu\left(\lambda + 2k_0 a\hat{Y}_S\right)}\,\mathrm{J}_{2m+2}(\nu)\,\mathrm{J}_{2n+2}(\nu)\,\mathrm{d}\nu \tag{42}$$

and

$$U_m^{(1)} = \frac{I_0 k_0 a R}{2}\int_0^\infty \frac{1}{\left(k_0 a + 2\lambda\hat{Z}_S\right)}\,\mathrm{e}^{-\mathrm{j}\lambda|h|/a} \cdot \mathrm{J}_1\left(\nu\frac{R}{a}\right)\mathrm{J}_{2m+2}(\nu)\,\mathrm{d}\nu \tag{43}$$

$$U_m^{(2)} = \zeta_0\frac{I_0 R}{2}\int_0^\infty \frac{1}{\left(\lambda + 2k_0 a\hat{Y}_S\right)}\,\mathrm{e}^{-\mathrm{j}\lambda|h|/a} \cdot \mathrm{J}_1\left(\nu\frac{R}{a}\right)\mathrm{J}_{2m+2}(\nu)\,\mathrm{d}\nu\,. \tag{44}$$

Once the system is solved, the coefficients $\psi_n^{(i)}$ furnish the unknown spectral currents through

$$\tilde{J}_{S\phi}\left(\frac{\nu}{a}\right) = \frac{1}{\beta_1(\nu)}\left[\sum_{n=0}^{+\infty}\psi_n^{(1)}\mathrm{J}_{2n+2}(\nu) + \nu G_1(\nu)\right] \tag{45}$$

and

$$\tilde{M}_{S\rho}\left(\frac{\nu}{a}\right) = \frac{1}{\beta_2(\nu)}\left[\sum_{n=0}^{+\infty}\psi_n^{(2)}\mathrm{J}_{2n+2}(\nu) + \nu G_2(\nu)\right]. \tag{46}$$

Such spectral currents can then be used to calculate any component of the field. In particular, the z-components of the scattered magnetic fields $H_z^{(1)\mathrm{scat}}$ and $H_z^{(2)\mathrm{scat}}$ for $z < 0$ are given by

$$H_z^{(1)\mathrm{scat}}(r,z) = -\frac{\mathrm{j}}{2a^2}\int_0^\infty \tilde{J}_{S\phi}\left(\frac{\nu}{a}\right)\frac{\mathrm{e}^{-\mathrm{j}\lambda|z|/a}}{\lambda}\,\mathrm{J}_0(\nu r)\,\nu^2\,\mathrm{d}\nu \tag{47}$$

and

$$H_z^{(2)\mathrm{scat}}(r,z) = -\frac{\mathrm{j}}{2k_0\zeta_0 a^3} \cdot \int_0^\infty \tilde{M}_{S\rho}\left(\frac{\nu}{a}\right)\mathrm{e}^{-\mathrm{j}\lambda|z|/a}\,\mathrm{J}_0(\nu r)\,\nu^2\,\mathrm{d}\nu \tag{48}$$

so that

$$H_z^{\mathrm{scat}}(r,z) = H_z^{(1)\mathrm{scat}}(r,z) + H_z^{(2)\mathrm{scat}}(r,z)\,. \tag{49}$$

The z-component of the magnetic field radiated by the original current loop source is instead

$$H_z^{\mathrm{inc}}(r,z) = -\mathrm{j}\frac{I_0 R}{2a^2}$$

$$\cdot \int_0^{\infty} \frac{\mathrm{e}^{-\mathrm{j}\lambda(h+|z|)/a}}{\lambda} \mathrm{J}_1\left(\nu\frac{R}{a}\right) \mathrm{J}_0\left(\nu r\right) \nu^2 \,\mathrm{d}\nu\,. \tag{50}$$

A. Field Calculation

Now, we consider the magnetic-field calculation along the z-axis, which is the critical case for shielding-effectiveness evaluations. Therefore, by assuming and suppressing $\rho = 0$ throughout, we have

$$H_z^{\mathrm{inc}}(z) = -\mathrm{j}\frac{I_0 R}{2a^2} \int_0^{\infty} \frac{\mathrm{e}^{-\mathrm{j}\lambda(h+|z|)/a}}{\lambda} \mathrm{J}_1\left(\nu\frac{R}{a}\right) \nu^2 \,\mathrm{d}\nu\,. \tag{51}$$

Moreover

$$H_z^{(1)\mathrm{scat}}(z) = -\frac{\mathrm{j}}{2a^2} \int_0^{\infty} \frac{1}{\beta_1(\nu)} \left[\sum_{n=0}^{+\infty} \psi_n^{(1)} \mathrm{J}_{2n+2}(\nu) + \nu G_1(\nu)\right] \frac{\mathrm{e}^{-\mathrm{j}\lambda|z|/a}}{\lambda} \nu^2 \,\mathrm{d}\nu \tag{52}$$

i.e.,

$$H_z^{(1)\mathrm{scat}}(z) = -\frac{\mathrm{j}}{a^2} \int_0^{\infty} \frac{2\nu}{\left(k_0 a + 2\hat{Z}_S \lambda\right)} \mathrm{e}^{-\mathrm{j}\lambda|z|/a} \left[\sum_{n=0}^{+\infty} \psi_n^{(1)} \mathrm{J}_{2n+2}(\nu) - I_0 k_0 a R \frac{\nu}{2\lambda} \mathrm{e}^{-\mathrm{j}\lambda|h|/a} \mathrm{J}_1\left(\nu\frac{R}{a}\right)\right] \mathrm{d}\nu \tag{53}$$

so that

$$H_z^{(1)\mathrm{scat}}(z) = H_z^{(1a)}(z) + H_z^{(1b)}(z) \tag{54}$$

with

$$H_z^{(1a)}(z) = -\frac{\mathrm{j}}{a^2} \sum_{n=0}^{+\infty} \psi_n^{(1)} \int_0^{\infty} \frac{\nu \,\mathrm{e}^{-\mathrm{j}\lambda|z|/a}}{\left(k_0 a + 2\hat{Z}_S \lambda\right)} \mathrm{J}_{2n+2}(\nu) \,\mathrm{d}\nu \tag{55}$$

and

$$H_z^{(1b)}(z) = \frac{\mathrm{j} I_0 k_0 R}{2a} \int_0^{\infty} \frac{\nu^2 \,\mathrm{e}^{-\mathrm{j}\lambda(h+|z|)/a}}{\lambda\left(k_0 a + 2\hat{Z}_S \lambda\right)} \mathrm{J}_1\left(\nu\frac{R}{a}\right) \mathrm{d}\nu. \tag{56}$$

Analogously

$$H_z^{(2)\mathrm{scat}}(z) = -\frac{\mathrm{j}}{2k_0\zeta_0 a^3} \int_0^{\infty} \frac{1}{\beta_2(\nu)} \left[\sum_{n=0}^{+\infty} \psi_n^{(2)} \mathrm{J}_{2n+2}(\nu) + \nu G_2(\nu)\right] \mathrm{e}^{-\mathrm{j}\lambda|z|/a} \nu^2 \,\mathrm{d}\nu \tag{57}$$

i.e.,

$$H_z^{(2)\mathrm{scat}}(z) = -\frac{\mathrm{j}}{2k_0\zeta_0 a^3} \int_0^{\infty} \frac{2k_0 a \nu^2 \,\mathrm{e}^{-\mathrm{j}\lambda|z|/a}}{\nu\left(\lambda + 2k_0 a \hat{Y}_S\right)} \cdot \left[\sum_{n=0}^{+\infty} \psi_n^{(2)} J_{2n+2}(\nu) - \nu\frac{I_0 R \zeta_0}{2} \mathrm{e}^{-\mathrm{j}\lambda|h|/a} \mathrm{J}_1\left(\nu\frac{R}{a}\right)\right] \mathrm{d}\nu \tag{58}$$

so that

$$H_z^{(2)\mathrm{scat}}(z) = H_z^{(2a)}(z) + H_z^{(2b)}(z) \tag{59}$$

where

$$H_z^{(2a)}(z) = -\frac{\mathrm{j}}{\zeta_0 a^2} \sum_{n=0}^{+\infty} \psi_n^{(2)} \int_0^{\infty} \frac{\nu \,\mathrm{e}^{-\mathrm{j}\lambda|z|/a}}{\left(\lambda + 2k_0 a \hat{Y}_S\right)} J_{2n+2}(\nu) \,\mathrm{d}\nu \tag{60}$$

and

$$H_z^{(2b)}(z) = \frac{\mathrm{j} I_0 R}{2a^2} \int_0^{\infty} \frac{\nu^2 \,\mathrm{e}^{-\mathrm{j}\lambda(|z|+h)/a}}{\left(\lambda + 2k_0 a \hat{Y}_S\right)} \mathrm{J}_1\left(\nu\frac{R}{a}\right) \mathrm{d}\nu. \tag{61}$$

By performing the change of variable $\kappa = \nu/a$ in (56) and (61) we obtain

$$H_z^{(1b)}(z) = \frac{\mathrm{j} I_0 R}{2k_0} \int_0^{\infty} \frac{\kappa^2 \,\mathrm{e}^{-\mathrm{j}k_0\sqrt{1-\kappa^2}\,(h+|z|)}}{\sqrt{1-\kappa^2}\left(1+2\hat{Z}_S\sqrt{1-\kappa^2}\right)} \mathrm{J}_1(\kappa R) \,\mathrm{d}\kappa \tag{62}$$

and

$$H_z^{(2b)}(z) = \frac{\mathrm{j} I_0 R}{2k_0} \int_0^{\infty} \frac{\kappa^2 \,\mathrm{e}^{-\mathrm{j}k_0\sqrt{1-\kappa^2}\,(|z|+h)}}{\left(\sqrt{1-\kappa^2} + 2\hat{Y}_S\right)} \mathrm{J}_1(\kappa R) \,\mathrm{d}\kappa\,, \tag{63}$$

respectively.

B. Identification of Aperture Penetration and Field Diffusion Contributions

It can now be noted that the contributions $H_z^{(1b)}$ and $H_z^{(2b)}$ do not depend on the radius a of the aperture and their sum coincide with the field scattered by a solid screen without apertures [18], [32]. Based on the above remarks, the sum of the incident field and of the contributions (56) and (61) can thus be interpreted as the *infinite solid screen* contribution to the total magnetic field for which a closed-form solution can be derived [18], [32], while the sum of (55) and (60) as the *aperture* contribution. Therefore, we can define the aperture field and magneto-conductive plate field contributions as

$$\begin{aligned} H_z^{\mathrm{ap}}(z) &= H_z^{(1a)\mathrm{scat}}(z) + H_z^{(2a)\mathrm{scat}}(z) \\ &= -\frac{\mathrm{j}}{a^2} \sum_{n=0}^{+\infty} \psi_n^{(1)} \int_0^{\infty} \frac{\nu \,\mathrm{e}^{-\mathrm{j}\lambda|z|/a}}{\left(k_0 a + 2\hat{Z}_S \lambda\right)} \mathrm{J}_{2n+2}(\nu) \,\mathrm{d}\nu \\ &\quad - \frac{\mathrm{j}}{\zeta_0 a^2} \sum_{n=0}^{+\infty} \psi_n^{(2)} \int_0^{\infty} \frac{\nu \,\mathrm{e}^{-\mathrm{j}\lambda|z|/a}}{\left(\lambda + 2k_0 a \hat{Y}_S\right)} \mathrm{J}_{2n+2}(\nu) \,\mathrm{d}\nu \end{aligned} \tag{64}$$

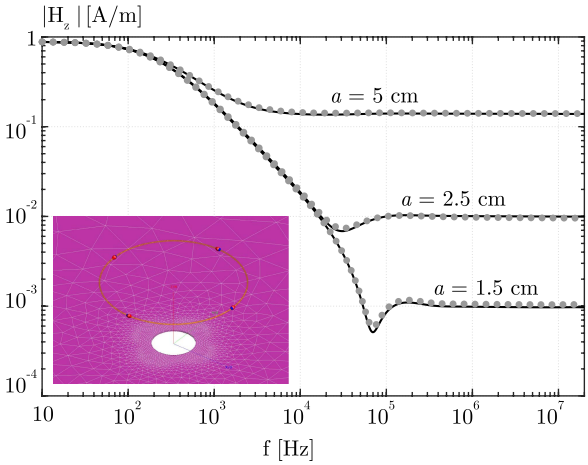

Fig. 3. Comparison between the proposed formulation (*black solid line*) and the results from FEKO (*gray dots*) as a function of frequency for different values of the aperture radius a. *Parameters:* $\sigma = 2.9 \cdot 10^7$ S/m, $\mu_r = 1$, $d = 1$ mm, $R = h = |z| = 5$ cm.

and

$$\begin{aligned} H_z^{\text{solid}}(z) &= H_z^{\text{inc}}(z) + H_z^{(1b)\text{scat}}(z) + H_z^{(2b)\text{scat}}(z) \\ &= -\text{j}\frac{I_0 R}{2k_0}\int_0^\infty \frac{\kappa^2\, \text{e}^{-\text{j}k_0\sqrt{1-\kappa^2}\,(h+|z|)}}{\sqrt{1-\kappa^2}}\,\text{J}_1(\kappa R)\,\text{d}\kappa \\ &\quad + \frac{\text{j}I_0 R}{2k_0}\int_0^\infty \frac{\kappa^2\, \text{e}^{-\text{j}k_0\sqrt{1-\kappa^2}(h+|z|)}}{\sqrt{1-\kappa^2}\left(1+2\hat{Z}_S\sqrt{1-\kappa^2}\right)}\text{J}_1(\kappa R)\,\text{d}\kappa \\ &\quad + \frac{\text{j}I_0 R}{2k_0}\int_0^\infty \frac{\kappa^2\, \text{e}^{-\text{j}k_0\sqrt{1-\kappa^2}\,(h+|z|)}}{\left(\sqrt{1-\kappa^2}+2\hat{Y}_S\right)}\text{J}_1(\kappa R)\,\text{d}\kappa\,, \end{aligned} \tag{65}$$

respectively.

Before presenting numerical results, we recall that magnetic shielding effectiveness SE_H is defined as

$$\text{SE}_H = 20\log\frac{\left|H_z^{\text{inc}}(z)\right|}{\left|H_z^{\text{solid}}(z)+H_z^{\text{ap}}(z)\right|}\,. \tag{66}$$

Analogously, we can define the SE of the solid screen and of the aperture as

$$\text{SE}^{\text{solid}} = 20\log\frac{\left|H_z^{\text{inc}}(z)\right|}{\left|H_z^{\text{solid}}(z)\right|} \tag{67}$$

and

$$\text{SE}^{\text{ap}} = 20\log\frac{\left|H_z^{\text{inc}}(z)\right|}{\left|H_z^{\text{ap}}(z)\right|}\,, \tag{68}$$

respectively.

IV. Numerical Results

The accuracy of the proposed numerical formulation is first checked by comparing its numerical results with those obtained through the commercial software Feldberechnung für Körper mit beliebiger Oberfläche (FEKO).

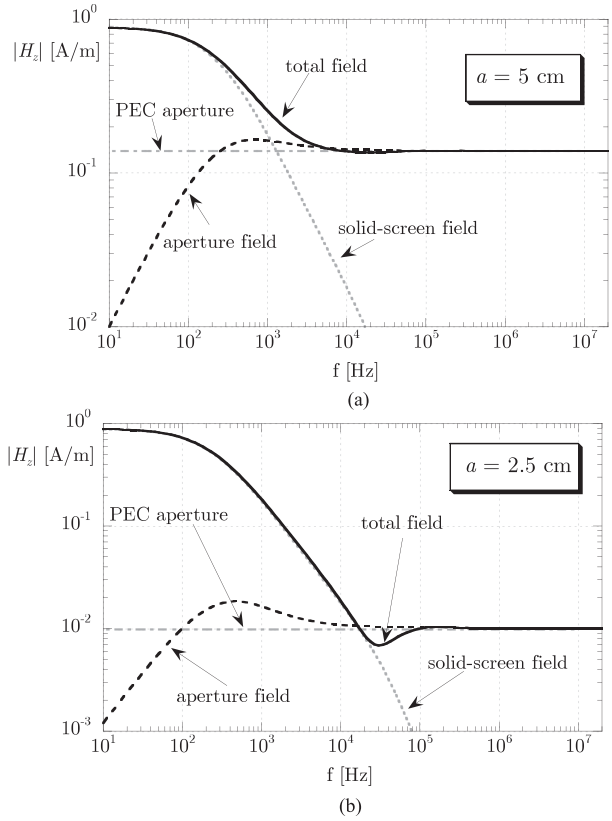

Fig. 4. Total magnetic-field contributions as a function of frequency. Parameters as in Fig. 2 with (a) $a = 5$ cm and (b) $a = 2.5$ cm.

A. Purely Conductive Screens

The first configuration consists of an electric current loop with current $I_0 = 1$ A of radius $R = 5$ cm coaxial with an aperture of radius a in a purely conductive screen with conductivity $\sigma = 2.9 \cdot 10^7$ S/m, relative permeability $\mu_r = 1$ (aluminum alloy), and thickness $d = 1$ mm. The electric current loop is placed at $h = R$. In Fig. 3, the absolute value of the z-component of the total magnetic field H_z is reported as a function of frequency from dc to 20 MHz at the observation point $z = -h$ for three different values of the aperture radius, i.e., $a = 1.5$ cm, $a = 2.5$ cm, and $a = 5$ cm. As it can be seen, there is a very good agreement between the results of the proposed exact formulation (*solid lines*) and those of FEKO (*gray dots*) . As shown in the inset of Fig. 3, the simulation through FEKO requires the accurate modeling of the source loop and aperture through suitable control of the mesh. The modeling of the source using several current ports placed along the loop does not allow to use symmetry planes. On a modern Intel desktop computer (I9-9900 K CPU, 64 GB RAM), the computational times range around 5 h over 301 frequency points using a mesh of 14.442 triangles with first order basis functions and double precision, while the proposed formulation takes only few seconds for each point.

The convergence properties of the exact formulation can be studied through the relative error ε_{err} between the the Nth and $(N+1)$th partial sums of the Neumann series in (34), as a function of N [21]. In general, very fast decrease of the relative error

ε_{err} can be observed, with a number of basis functions N which obviously depends on the involved geometrical and physical parameters. In the cases of Fig. 3, $N = 15$ basis functions have been used to obtain a relative error ε_{err} less than 10^{-3}.

As it can be seen, at low frequencies the level of the transmitted field is the same in all the aperture cases, while, by increasing frequency, the transmitted field in the case of the largest aperture ($a = 5$ cm) is much larger than in the other cases. To better understand the underlying physical mechanism, in Fig. 4 the contributions of the infinite-plate field H_z^{solid} and the aperture field H_z^{ap} to the total magnetic field are reported in the case of $a = 5$ cm (a) and $a = 2.5$ cm (b). Since the solid screen, the excitation configuration, and the observation point are the same in both the cases, the solid-screen field contribution is also the same and what is different is the aperture-field contribution, which is larger in the largest aperture case, as expected. In Fig. 4, for a fair comparison, the field transmitted through an aperture in a PEC screen is also reported [6]. As it can be seen this is the limiting case for large frequencies and it coincides with the aperture-field contribution. In practice, at low frequencies, the magnetic field is dominated by the solid-screen contribution(i.e., the same screen without any aperture) while at high frequencies is dominated by the aperture contribution (and, for very high frequencies it coincides with the magnetic field penetrating the same aperture in a PEC screen). However, in the intermediate frequency range, there is a transition region where both the contributions are important and shape the total transmitted magnetic field.

Finally, Fig. 5 shows the magnetic shielding effectiveness SE_H, SE^{plate}, and SE^{ap} for the same configurations. It can thus be seen that in the low-frequency range, since the contribution of the aperture field is negligible, the magnetic SE coincides with that of a solid screen with the same parameters. However, by increasing frequency, the aperture-field contribution becomes more important and this strongly limits the values of the SE. Obviously, in the case of a smaller aperture the maximum SE (which is obtained at high frequencies) is larger.

Dual results are obtained by changing the thickness of the plate. In fact this mainly influences the solid-screen contribution negligibly affecting the aperture contribution, so that for smaller thickness the transition region is reached at lower frequencies. The relevant results are not reported here for conciseness.

B. Magneto-Conductive Screens

The second configuration consists of the same setup considered in the previous section, but with a magneto-conductive screen (iron) having conductivity $\sigma = 1.8 \cdot 10^6$ S/m, relative permeability $\mu_{\text{r}} = 500$ (and again thickness $d = 1$ mm). In Fig. 6, the absolute value of the z-component of the total magnetic field H_z is reported as a function of frequency from dc to 20 MHz at the observation point $z = -h$ for $a = 1.5$ cm, $a = 2.5$ cm, and $a = 5$ cm. As in the case of purely conductive screens, there is a very good agreement between the results of the proposed exact formulation (*solid lines*) and those of FEKO (*gray dots*).

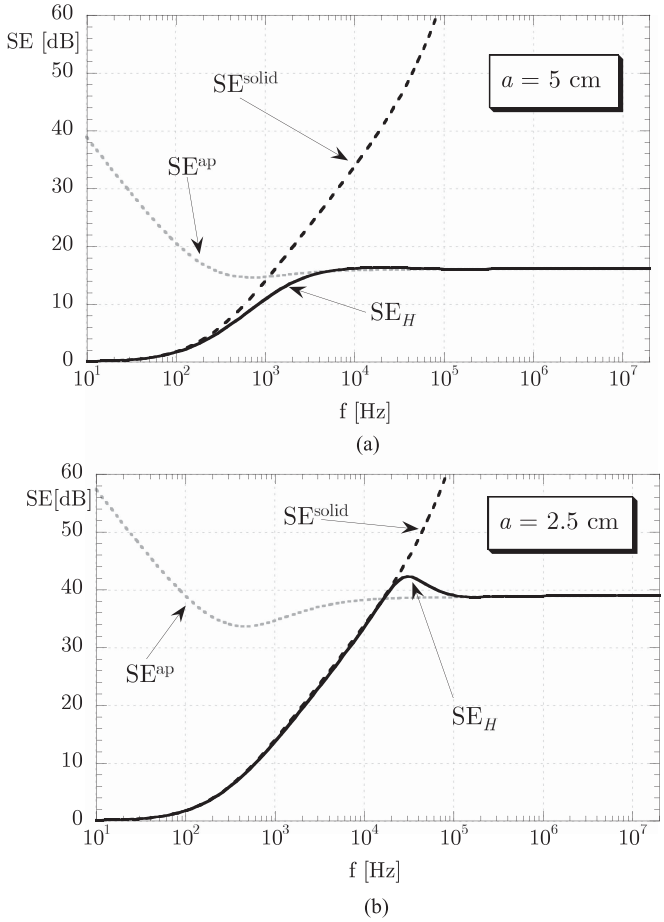

Fig. 5. Magnetic shielding-effectiveness as a function of frequency. Parameters as in Fig. 2 with (a) $a = 5$ cm and (b) $a = 2.5$ cm.

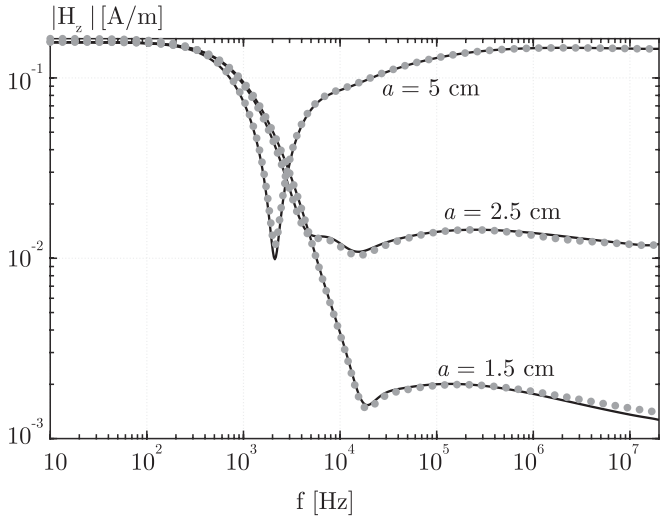

Fig. 6. Comparison between the proposed formulation (*black solid line*) and the results from FEKO (*gray dots*) as a function of frequency for different values of the aperture radius a. *Parameters:* $\sigma = 1.8 \cdot 10^6$ S/m, $\mu_{\text{r}} = 500$, $d = 1$ mm, $R = h = |z| = 5$ cm.

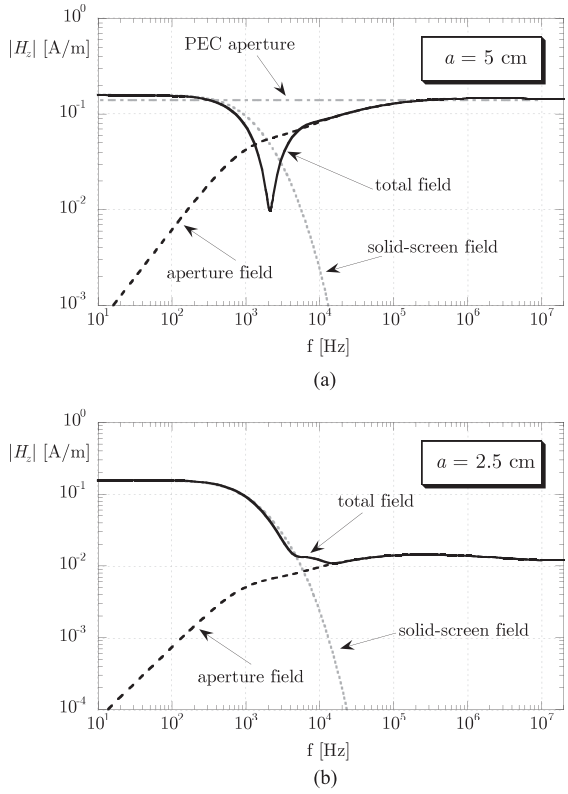

Fig. 7. Total magnetic-field contributions as a function of frequency. Parameters as in Fig. 6 with $a = 5$ cm (a) and $a = 2.5$ cm (b).

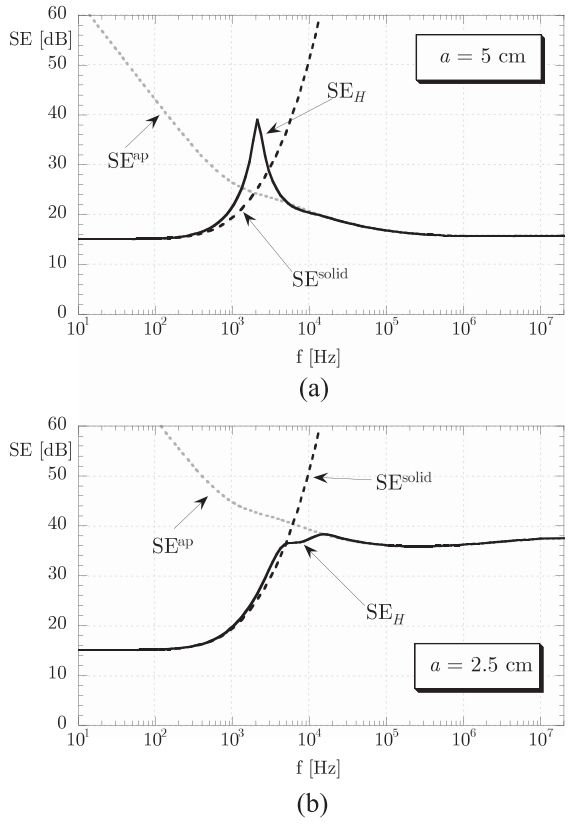

Fig. 8. Magnetic shielding-effectiveness as a function of frequency. Parameters as in Fig. 6 with $a = 5$ cm (a) and $a = 2.5$ (b).

For these configurations $N = 9$ basis functions have been used in order to obtain a relative error ε_{err} less than 10^{-3}.

In Fig. 7, the contributions of the solid-screen field H_z^{solid} and the aperture field H_z^{ap} to the total magnetic field are reported for the cases $a = 5$ cm and $a = 2.5$ cm. In the case of magneto-conductive screen, the transmitted magnetic-field at low frequencies is much smaller (because of the presence of a large permeability) and this makes the relevant solid-screen contribution much smaller and comparable with the aperture contribution thus determining, e.g., a destructive interference of the two contributions around $f = 2$ kHz in the case of $a = 5$ cm.

Finally, in Fig. 8, the magnetic shielding effectiveness SE_H, SE^{solid}, and SE^{ap} for the two configurations are reported. It can be seen that the destructive interference in the case $a = 5$ cm gives rise to an unexpected increasing of the SE in the kHz region, also with respect to the solid screen.

V. Conclusion

The diffusion and penetration of the magnetic field generated by a circular electric current loop through a coaxial circular aperture in a magneto-conductive screen of finite thickness is studied through an original formulation based on generalized boundary conditions and dual integral equations. The magnetic shielding effectiveness is studied in different configurations pointing out possible critical situations. Numerical results are also compared with those obtained through commercial software to show the accuracy and the efficiency of the proposed formulation. One remarkable advantage of the proposed formulation is that it allows for clearly distinguishing the contribution of the magnetic-field diffusion through the solid screen and of the penetration through the aperture thus gaining physical insight into the shielding performance. The relative weight of such contributions strongly depends on all the parameters of the considered configuration and it will be the subject of a future investigation.

References

[1] C. Flammer, "The vector wave function solution of the diffraction of electromagnetic waves by circular disks and apertures. II. The diffraction problems," *J. Appl. Phys.*, vol. 24, no. 9, pp. 1224–1231, Sep. 1953.

[2] H. A. Bethe, "Theory of diffraction by small holes," *Phys. Rev.*, vol. 66, no. 7-8, p. 163, pp. 163–182, Oct. 1944.

[3] C. J. Bouwkamp, "On the diffraction of electromagnetic waves by small circular disks and holes," *Philips Res. Rep.*, vol. 5, pp. 401–422, 1950.

[4] K. A. Michalski and J. R. Mosig, "On the plane wave-excited subwavelength circular aperture in a thin perfectly conducting flat screen," *IEEE Trans. Antennas Propag.*, vol. 62, no. 4, pp. 2121–2129, Apr. 2014.

[5] M. A. Christou and A. C. Polycarpou, "A Gegenbauer polynomial solution for the electromagnetic scattering by a subwavelength circular aperture in an infinite conducting screen," *Prog. Electromagn. Res.*, vol. 92, pp. 71–85, 2019.

[6] G. Lovat, P. Burghignoli, R. Araneo, and S. Celozzi, "Magnetic field penetration through a circular aperture in a perfectly conducting plate excited by a coaxial loop," *IET Microw. Antennas Propag.*, vol. 15, no. 10, pp. 1147–1158, 2021.

[7] M. Lucido, G. Panariello, and F. Schettino, "Scattering by a zero-thickness PEC disk: A new analytically regularizing procedure based on Helmholtz decomposition and Galerkin method," *Radio Sci.*, vol. 52, no. 1, pp. 2–14, Jan. 2017.

[8] G. Lovat et al., "Shielding of a perfectly conducting disk: Exact and static analytical solution," *Prog. Electromagn. Res. C*, vol. 95, pp. 167–182, 2019.

[9] A. Roberts, "Electromagnetic theory of diffraction by a circular aperture in a thick, perfectly conducting screen," *J. Opt. Soc. Amer. A*, vol. 4, no. 10, pp. 1970–1983, Oct. 1987.
[10] F. G. De Abajo, "Light transmission through a single cylindrical hole in a metallic film," *Opt. Exp.*, vol. 10, no. 25, pp. 1475–1484, 2002.
[11] H. S. Lee and H. J. Eom, "Electromagnetic scattering from a thick circular aperture," *Microw. Opt. Technol. Lett.*, vol. 36, no. 3, pp. 228–231, 2003.
[12] R. Wannemacher, "Plasmon-supported transmission of light through nanometric holes in metallic thin films," *Opt. Commun.*, vol. 195, no. 1-4, pp. 107–118, 2001.
[13] V. Bordo, "Ab *initio* analytical model of light transmission through a cylindrical subwavelength hole in an optically thick film," *Phys. Rev. B*, vol. 84, no. 7, 2011, Art. no. 075465.
[14] Z. Zhang, X. Yang, C. Jiao, Y. Yang, and J. Wang, "Analytical model for low-frequency magnetic field penetration through a circular aperture on a perfect electric conductor plate," *IEEE Trans. Electromagn. Compat.*, vol. 63, no. 5, pp. 1599–1604, Oct. 2021.
[15] J. R. Moser, "Low-frequency low-impedance electromagnetic shielding," *IEEE Trans. Electromagn. Compat.*, vol. 30, no. 3, pp. 202–210, Aug. 1988.
[16] R. C. Hansen and J. R. Moser, "Loop-shield-loop shielding effectiveness," *IEEE Trans. Electromagn. Compat.*, vol. 41, no. 2, pp. 144–146, May 1999.
[17] G. Lovat, P. Burghignoli, R. Araneo, and S. Celozzi, "Magnetic shielding of planar metallic screens: A new analytical closed-form solution," *IEEE Trans. Electromagn. Compat.*, vol. 62, no. 5, pp. 1884–1888, Oct. 2020.
[18] G. Lovat, P. Burghignoli, R. Araneo, E. Stracqualursi, and S. Celozzi, "Analytical evaluation of the low-frequency magnetic shielding of thin planar magnetic and conductive screens," *IEEE Trans. Electromagn. Compat.*, vol. 63, no. 1, pp. 308–312, Feb. 2021.
[19] G. Lovat, P. Burghignoli, R. Araneo, E. Stracqualursi, and S. Celozzi, "Closed-form LF magnetic shielding effectiveness of thin planar screens in coplanar loops configuration," *IEEE Trans. Electromagn. Compat.*, vol. 63, no. 2, pp. 631–635, Apr. 2021.
[20] C. Jiao et al., "Low-frequency magnetic shielding of planar shields: A unified wave impedance formula for the transmission line analogy," *IEEE Trans. Electromagn. Compat.*, vol. 63, no. 4, pp. 1046–1057, Aug. 2021.
[21] G. Lovat, P. Burghignoli, R. Araneo, and S. Celozzi, "Axially symmetric source field penetration through a circular aperture in a thin impedance plate," *IEEE Trans. Antennas Propag.*, vol. 70, no. 9, pp. 8348–8359, Sep. 2022.
[22] O. V. Shapoval, R. Sauleau, and A. I. Nosich, "Scattering and absorption of waves by flat material strips analyzed using generalized boundary conditions and Nystrom-type algorithm," *IEEE Trans. Antennas Propag.*, vol. 59, no. 9, pp. 3339–3346, Sep. 2011.
[23] I. O. Sukharevsky, O. V. Shapoval, A. Altintas, and A. I. Nosich, "Validity and limitations of the median-line integral equation technique in the scattering by material strips of sub-wavelength thickness," *IEEE Trans. Antennas Propag.*, vol. 62, no. 7, pp. 3623–3631, Jul. 2014.
[24] M. Lucido, M. V. Balaban, S. Dukhopelnykov, and A. I. Nosich, "A fast-converging scheme for the electromagnetic scattering from a thin dielectric disk," *Electronics*, vol. 9, no. 9, 2020, Art. no. 1451.
[25] M. Lucido, F. Schettino, and G. Panariello, "Scattering from a thin resistive disk: A guaranteed fast convergence technique," *IEEE Trans. Antennas Propag.*, vol. 69, no. 1, pp. 387–396, Jan. 2021.
[26] M. Lucido, M. V. Balaban, and A. I. Nosich, "Plane wave scattering from thin dielectric disk in free space: Generalized boundary conditions, regularizing Galerkin technique and whispering gallery mode resonances," *IET Microw. Antennas Propag.*, vol. 15, no. 10, pp. 1159–1170, 2021.
[27] K. Mitzner, "Effective boundary conditions for reflection and transmission by an absorbing shell of arbitrary shape," *IEEE Trans. Antennas Propag.*, vol. 16, no. 6, pp. 706–712, Nov. 1968.
[28] A. Karlsson, "Approximate boundary conditions for thin structures," *IEEE Trans. Antennas Propag.*, vol. 57, no. 1, pp. 144–148, Jan. 2009.
[29] T. B. A. Senior and J. L. Volakis, *Approximate Boundary Conditions in Electromagnetics*. London, U.K.: IET, 1995.
[30] W. C. Chew, *Waves and Fields in Inhomogenous Media*. Piscataway, NJ, USA: IEEE Press, 1999.
[31] I. S. Gradshteyn and I. M. Ryzhik, *Table of Integrals, Series, and Products*. 7th ed.New York, NY, USA: Academic, 2014.
[32] G. Lovat, P. Burghignoli, R. Araneo, and S. Celozzi, "Exact closed-form shielding effectiveness of planar screens with small parallel loops," *IEEE Trans. Electromagn. Compat.*, vol. 64, no. 5, pp. 1694–1702, Oct. 2022.